Microwave Radiometer Measurement of Water Vapor Path Delay: Data Reduction Techniques

E. S. Claflin, S. C. Wu, and G. M. Resch
Tracking Systems and Applications Section

Unmodeled electrical path delay from atmospheric water vapor is a limiting error source in geodetic measurements made with very long baseline interferometry and in radio ranging to spacecraft. A dual channel water vapor radiometer, operating near the 22.235-GHz water vapor line, is capable of measuring water vapor-induced delay with good accuracy under most weather conditions. Theory shows that water vapor path delay ΔL_v is proportional to a linear combination of saturation-corrected sky brightness temperatures, measured on and off the water vapor line. The second, off-line, channel removes the effects of emission from liquid water droplets in clouds as well as most of the oxygen emission. Tipping curves remove instrumental error. Sky brightness temperatures are saturation-corrected or "linearized" using estimates of effective sky temperature made from surface temperature. Coefficients in the expression for path delay ΔL_v are functions of surface temperature, pressure, and water vapor density, allowing use of our data reduction algorithm at any altitude and in any climate. Coefficients are found by two methods: (1) from a regression analysis of measured brightness temperatures versus radiosonde measured delay, and (2) from a regression of theoretical brightness temperatures versus radiosonde measured delay. Regression solutions are constrained to remove liquid water contributions and to give the correct slope (i.e., one) for radiometer versus radiosonde path delay.

I. Introduction

Very long baseline interferometry (VLBI) and other extra-terrestrial, microwave, geodetic techniques have potential accuracies at the few centimeter level (Ref. 1). Propagation media effects constitute a limiting error source, however, and must be compensated for to achieve the highest accuracy otherwise inherent in present and planned systems. In particular, one must devise a way to compensate for tropospheric water vapor. Water vapor induced path delay in the zenith direction can vary from less than 1 to more than 30 centimeters depending on climate and weather.

Under favorable conditions, water vapor delay can be solved for as part of the final fitting of residuals in the VLBI data reduction process. If baseline geometry is not favorable, the solve-for procedure will degrade accuracy appreciably.

Moreover, the solve-for solution breaks down if changes in water vapor delay occur rapidly or if the atmosphere has large horizontal inhomogeneities. An independent way to measure delay from tropospheric water vapor is needed.

From among a number of candidate measuring techniques, we have found that the most satisfactory is passive microwave radiometry. A microwave radiometer will operate day or night and under all weather conditions except rain or heavy snow. Spatially, measurements can be made in all directions that are more than a few beamwidths from the horizon and from the sun. Microwave radiometry will, in the future, also be applicable to VLBI geodesy with satellite radio sources and to radio ranging for navigation of interplanetary spacecraft. The purpose of this paper is to present techniques for conversion of radiometer data to water vapor path delay. A discussion of errors will be presented in a later paper.

II. Background

A solution of the radiative transfer equation governing propagation of microwave radiation downward through a nonscattering atmosphere in thermodynamic equilibrium is (Ref. 2)

$$T_B = T_c\, e^{-\tau(\infty)} + \int_0^\infty T\alpha\, e^{-\tau(s)}\, ds \qquad (1)$$

where

$$\tau(s) = \int_0^s \alpha\, ds$$

is the optical depth, α is the absorption coefficient (distance^{-1}), s is distance upward along the signal path, T is physical temperature of the air, T_B is the sky brightness temperature, and T_c is the cosmic blackbody temperature of about 2.8 K. Typical half-power antenna beamwidths of 5 to 10 degrees are large enough that all celestial sources of radiation are negligible except for the sun.

Important contributions to α are made by atmospheric water vapor, oxygen, and the liquid water droplets in clouds or fog. Water vapor has a spectral line at 22.235 Ghz. Sensitivity to water vapor is achieved by choosing a primary frequency on or near this line. The liquid water contribution from clouds is removed by using a second frequency channel and then linearly combining sky temperatures from both channels. We find that it is sufficiently accurate to assume an f^2 frequency dependence for the liquid water absorption coefficient.[1] The oxygen contribution is from a complex of spectral lines near 60 GHz and has a frequency dependence which is also approximately f^2. About 82 percent of the oxygen contribution is removed by the f^2 dependence assumed for liquid emission. This is fortuitous because oxygen emission also depends on atmospheric temperature, a quantity subject to estimation error. The remaining 18 percent of the oxygen contribution is removed by a small term proportional to air mass in the expression for water vapor path delay. At one air mass this term is approximately −0.4 cm path delay.

A related matter that has already been investigated in some detail is optimal choice of frequency pair for the two radiometer channels. To retrieve water vapor path delay with highest accuracy, it is necessary to use a frequency pair which minimizes error from all sources. No single frequency pair is ideal under all conditions; however, we recognize that a very important consideration is that a frequency pair be chosen which minimizes variation with altitude of the weighting function $W'(s)$ (Ref. 3):

$$W'(s) = \frac{T(T - T_c)}{\rho}\left[\frac{\alpha_{v,1}}{f_1^2} - \frac{\alpha_{v,2}}{f_2^2}\right] \qquad (2)$$

where α_v is the absorption coefficient for water vapor and ρ is water vapor density. The penalty for a nonconstant Eq. (2) along the observing path is appreciable error whenever the water vapor altitude distribution varies markedly from some calibration distribution. Such variations appear to be most common in coastal regions, where layering of marine and continental air is a frequent occurrence. Optimal choice of frequency pairs has been discussed by Wu (Ref. 3). Frequency pairs of 20.3/31.4, 20.0/26.5, and 24.5/31.4 GHz are all near optimal for minimizing variations in weighting function (Eq. 2) with altitude.

[1] Liquid water absorption coefficient frequency dependence was calculated for the case of droplets small compared with wavelength (Rayleigh scattering). The dependence is very nearly f^2, but is slightly affected by temperature (Refs. 4, 5). For a 22.235/31.4-GHz frequency pair, deviations from f^2 behavior will cause an error in path delay of less than 0.7 cm even under the extreme conditions of 1000 μm liquid water, 20-degree elevation angle, and temperature of 0°C. Note also that path delay from liquid water is negligible; 1000 μm of vertical columnar liquid water at 20-degree elevation angle causes path delay of less than 0.5 cm (Ref. 6). For a next generation system, these effects could be estimated to refine the total delay correction.

III. Outline of Technique

The data reduction system developed here can be separated into two parts or activities. The first part comprises techniques for converting raw radiometer data and surface temperature into linearized sky brightness temperatures. An important element of this procedure is the use of tipping curves to provide an instrumental calibration.

The second part is calculation of suitable coefficients for use in finding path delay. Two methods will be discussed for calculating coefficients, both using a regression analysis. In each case the coefficients are adjusted for differing climatic conditions by measurements of surface temperature, pressure, and relative humidity.

IV. Linearized Brightness Temperature and Water Vapor Path Delay

Presence of the exponential terms in Eq. (1) prevents sky brightness temperature from increasing linearly with increasing water vapor path delay. In the limit of small opacities, the relation *is* linear. In the limit of extremely high opacities, sky brightness temperature becomes equal to surface atmospheric temperature (saturates) and is completely insensitive to changes in water vapor path delay. Between these limits it is possible to "linearize" (saturation-correct) brightness temperature. The purpose of linearization is to transform the calculation of path delay into the familiar problem of solving two linear equations in two unknowns. (The two unknowns are water vapor path delay and integrated liquid water.)

If the linearized brightness temperature T'_B is defined by

$$T'_B = T_c\,[1 - \tau(\infty)] + \int_0^\infty T\alpha\, ds$$

$$= T_c + \int_0^\infty (T - T_c)\,\alpha\, ds \qquad (3)$$

then linearized brightness temperature may be calculated from measured brightness temperature T_B using the following relation derived from Eqs. (1) and (3) (Ref. 3):

$$T'_B = T_c - (T'_{eff} - T_c)\ln\left(1 - \frac{T_B - T_c}{T_{eff} - T_c}\right) \qquad (4)$$

with

$$T_{eff} = \frac{\int_0^\infty T\,\alpha\, e^{-\tau(s)}\, ds}{\int_0^\infty \alpha\, e^{-\tau(s)}\, ds} \qquad (5)$$

$$T'_{eff} = \frac{\int_0^\infty T\,\alpha\, ds}{\int_0^\infty \alpha\, ds} \qquad (6)$$

For small opacities, $T'_{eff} \approx T_{eff}$. For large zenith opacities or small elevation angles, $T'_{eff} < T_{eff}$. Since atmospheric temperature is readily accessible only at the ground, surface values must be used to estimate T_{eff}. A simple expression

$$T_{eff} = T'_{eff} = k_e T \qquad (7)$$

(where T is absolute surface temperature) is sufficient for dry climates. k_e is a function of frequency and can be found by integrating radiosonde profiles with Eq. (6). Typically $0.92 < k_e < 0.95$. More accurate, but more complex, schemes for estimating T_{eff} and T'_{eff} can be devised.

T'_B, the linearized brightness temperature, is not very sensitive to T_{eff} and T'_{eff}. Figure 1 shows the linearization correction $T'_B - T_B$ as a function of T_B for three different estimates of $T_{eff} = T'_{eff}$. The correction becomes a significant error source only at very high sky temperatures. Observed zenith sky brightness temperatures at 22.235 GHz have been in the range 13 to 100 K. At 31.4 GHz the range has been 11 to 45 K. The corresponding range of zenith path delays covered by these observations was from 2 to 30 cm.

Wu (Ref. 3) has shown that for a dual channel radiometer, path delay is given by

$$\Delta L_v = (b'_0 + b_1 T'_{B,1} + b_2 T'_{B,2})/W'(0) \qquad (8)$$

where

$$b'_0 = Gb_0 - T_c(b_1 + b_2) \qquad (9)$$

$$G = m(P/\bar{P})^2\,(\bar{T}/T)^{1.85} \qquad (10)$$

b_0, b_1, b_2 = constants

P = surface pressure: force/area

T = surface temperature

$T'_{B,1}$ and $T'_{B,2}$ are derived from measured brightness temperatures at the two frequencies using Eq. (4). $W'(0)$ is the weighting function of Eq. (2) evaluated at the surface to adjust path delay for varying values of surface temperature, pressure, and water vapor density. The variable G adjusts for changes in air mass m and for changes in the oxygen absorption coefficient with changes in surface temperature and pressure. $\overline{T}$ and $\overline{P}$ are nominal surface values, but are best chosen to be representative of the calibrating or operating conditions. Expressions for the water vapor absorption coefficient α_v can be found in Waters (Ref. 2) and Westwater (Ref. 7). The coefficients b_0, b_1, b_2 can be determined either from theory and a suitable ensemble of radiosonde profiles or from regression of measured sky temperatures against path delays from simultaneous radiosonde data. These methods will be discussed in a later section.

For convenient routine application, Eqs. (8), (9), and (10) can be written as

$$\Delta L_v = a'_0 m - T'_c + a_1 T'_{B,1} + a_2 T'_{B,2} \tag{11}$$

$$a'_0 = \frac{b_0 (P/\overline{P})^2 (\overline{T}/T)^{1.85}}{W'(0)} \tag{12}$$

$$T'_c = \frac{T_c(b_1 + b_2)}{W'(0)} \tag{13}$$

$$a_1 = b_1/W'(0) \tag{14}$$

$$a_2 = b_2/W'(0) \tag{15}$$

and a table of coefficients a'_0, T'_c, a_1, a_2 prepared for suitable choices of P, T, and ρ values. We have found that sufficient resolution is provided by increments of 20 mb (2000 N/m^2) in P, 10°C in T, and relative humidities of 20, 50 and 80 percent.

V. Measurement of Sky Brightness Temperature

Radiometer output is an analog signal which varies linearly with input signal power. Since the constant of proportionality is gain dependent, every radiometer contains two reference loads at carefully measured physical temperatures to establish a brightness temperature calibration. If the sky brightness temperature is T_B, the ambient or base load temperature T_A, and the hot load temperature T_H, then the corresponding number of counts N_B, N_A, N_H (from an analog to digital converter) are related to brightness temperature by

$$T_B = T_A + (T_H - T_A)\gamma \tag{16}$$

$$\gamma = (N_B - N_A)/(N_H - N_A) \tag{17}$$

In practice Eq. (16) is imperfect because of losses and reflections in the horn, waveguide, and switching system. Figure 2 shows typical switches and signal paths for a radiometer. T^*_B, T^*_H, T^*_A are apparent brightness temperatures at the common input. We assume *a priori* that switch isolation is very good (typically the isolation is ~30 dB). Then

$$T^*_B = T_B \beta_B + T_{BL} \tag{18}$$

$$T^*_H = T_H \beta_H + T_{HL} \tag{19}$$

$$T^*_A = T_A \tag{20}$$

are expressions for the input temperatures for a simple linear model in which the input signal suffers attenuation β_i and receives augmentation T_{iL}. The β_i's and T_{iL}'s are temperature dependent. Temperature stabilization of the instrument should remove most of the variation in these parameters. Equation (20) assumes that the switch and waveguide temperatures are nearly the same as the ambient load temperature T_A.

Solving Eqs. (16), (18), (19), and (20) for T_B,

$$T_B = \beta_B^{-1} \left[(T_A - T_{BL}) + (T_H \beta_H + T_{HL} - T_A)\gamma \right] \tag{21}$$

Determination of the four instrumental constants β_B, β_H, T_{BL}, and T_{HL} is not straightforward either theoretically or experimentally. A simplified version of Eq. (21) can be written by assuming $\beta_B \simeq 1$ and $T_{BL} \simeq 0$, which implies negligible losses and reflections between antenna and receiver input. The instrumental constants are then replaced by the "hot load correction," $\Delta T_H = T_H(\beta_H - 1) + T_{HL}$, so that

$$T_B = T_A + (T_H + \Delta T_H - T_A)\gamma \tag{22}$$

The single constant ΔT_H can be found by performing "tipping curves" as outlined in the following section. Some variation in ΔT_H will occur with different brightness and physical temperatures because Eq. (22) is only an approximation to Eq. (21).

VI. Tipping Curves and the Hot Load Correction

Tipping curves are performed by taking measurements of sky brightness temperature at several elevation angles. When a straight line is fitted to linearized brightness temperatures from Eqs. (22) and (4) as a function of air mass, the expected intercept at zero air mass is T_c. Suppose the intercept has a different value $T'_B(0)$. ΔT_H must be adjusted to achieve the desired intercept. Figure 3 shows a straight line fit before (dashed) and after (solid) adjustment of ΔT_H. (The two lines intersect off the graph at $T'_B = T'_A$.)

If the hot load correction is initially taken to be zero, then one can show that

$$\Delta T_H = \frac{[T_c - T'_B(0)]\ [T_H - T_A]}{[T'_B(0) - T_A]} \tag{23}$$

is a good estimate of the required hot load correction. Corresponding sky brightness temperature correction is found from Eq. (22) to be

$$\Delta T_B = \Delta T_H \left(\frac{T_B - T_A}{T_H - T_A} \right) \tag{24}$$

New sky brightness temperatures $T_B + \Delta T_B$ are linearized with Eq. (4) and fitted again to a straight line. The process is repeated[2] as many times as necessary to adjust $T'_B(0)$, the intercept, to within about 0.1 K of T_c. Normally two or three iterations are sufficient. We generally use three points at 1, 1.5, and 2 air masses (90-, 42-, and 30-degree elevation angles) for tipping curves. Repeating the measurement at four points of the compass (different azimuths) provides redundancy in the data and averages over spatial gradients.

Various problems with the measurement system can cause a poor tipping curve. Quality criteria for a tipping curve are the value of the linear correlation coefficient, the size of the hot load correction and its agreement with a "historical" estimate, and the agreement of the estimated zenith path delay with those derived from tipping curves at other azimuths.

Experience with an instrument will show to what degree ΔT_H is constant for each channel. One can then estimate error incurred by using nominal values of ΔT_H to replace tipping curves.

In principle, the most meaningful delay is found by measurements along the line-of-sight to the radio source being observed. For an automated system, a horizon mask for each site and a solar ephemeris are needed to avoid pointing the instrument toward contaminating radiation. Under dry conditions, pointing along the line-of-sight is not likely to give measurable improvement over extrapolated zenith values. In fact, error may be introduced by sidelobe pickup and poorer performance of the data reduction algorithm at low elevation angles. We expect pointing to improve VLBI results under very humid, cloudy conditions.

VII. Coefficient Determination: Regression of Sky Brightness Temperatures Versus Radiosonde Path Delay

Water vapor delay is computed from a radiosonde profile with the expression (Refs. 8 and 9).

$$\Delta L'_v = (1.723 \times 10^{-3}\ \text{K-m}^3/\text{g}) \int_0^\infty \rho/T\, ds \tag{25}$$

where the prime indicates a radiosonde measurement.

---

[2] Equations (23) and (24) must be generalized slightly to take into account each new adjustment of the hot load temperature T_H.

If

$$T_{Hi} = T_H + \Delta T_{Hi}$$

$$\Delta T_{Hi} = \sum_{j=0}^{i} \Delta T_{Hj}^{\text{inc}}$$

and

$$\Delta T_{H0}^{\text{inc}} = 0$$

then

$$\Delta T_{H(i+1)}^{\text{inc}} = \frac{[T_c - T'_B(0)_i]\ [T_{Hi} - T_A]}{[T'_B(0)_i - T_A]} \tag{23a}$$

$$\Delta T_{B(i+1)} = \Delta T_{H(i+1)} \left(\frac{T_B - T_A}{T_H - T_A} \right) \tag{24a}$$

where $i = 0, 1, 2, \ldots$ is the iteration number and "inc" is incremental change.

Suppose a suitably representative group of radiosonde launches has been made, and sky brightness temperatures measured with a radiometer at the time of each launch. The coefficients b_0, b_1, b_2 of Eq. (8) and Eq. (9) may be found by minimizing:

$$S = \sum_i (\Delta L_{vi} - \Delta L'_{vi})^2 \qquad (26)$$

with respect to b_0, b_1, and b_2, but subject to several constraints.

The first constraint ensures that background contributions are eliminated:

$$b_1/b_2 = -(f_2/f_1)^2 \qquad (27)$$

Two more constraints enforce unity slope and zero intercept on the best-fit straight line of radiometer-measured to radiosonde-measured path delays:[3]

$$\sum_i \Delta L_{vi} = \sum_i \Delta L'_{vi} \qquad (28)$$

$$\sum_i (\Delta L_{vi})(\Delta L'_{vi}) = \sum_i (\Delta L'_{vi})^2 \qquad (29)$$

If these constraints are not used, slope and intercept may vary appreciably from 1 and 0. This unphysical result is a necessary consequence of random measurement error in sky brightness temperatures and in radiosonde-measured path delays: Scatter in the residuals of Eq. (26) will be minimized by values of b_1 and b_2 which are too small, offset by a value of b_0 which is too large. Figures 4A and 4B illustrate fits obtained with and without constraints on slope and intercept. The coefficients of Fig. 4B will predict too much water vapor path delay under dry conditions and too little under wet conditions.

[3]One may show that only the constraint on slope is actually required. In practice it is easier to constrain both slope and intercept.

Lagrange multipliers may be used to minimize Eq. (26) with respect to b_0, b_1, b_2, but subject to the constraints of Eqs. (27), (28), (29). The problem is thereby simplified to a set of six linear equations in six unknowns. The regression may also be carried out without actual measurement of sky brightness temperatures. Linearized brightness temperatures can be calculated from Eq. (3) using the water vapor absorption coefficient of Waters (Ref. 2) or Westwater (Ref. 7) and the oxygen absorption coefficient of Westwater (Ref. 7).[4] As before, one uses a representative sample of radiosonde profiles.

There is sufficient uncertainty in the water vapor absorption coefficient to cast some doubt on the accuracy of results obtained by the theoretical method. Nevertheless, we have found that the theoretical method gives coefficients in fairly good agreement with those obtained by regression against measured brightness temperatures.

VIII. Summary

A systematic method for reducing dual-frequency water vapor radiometer data to water vapor path delay has been developed. Linearized sky brightness temperatures and path delay coefficients are computed in separate procedures and then combined to calculate path delay. Sky brightness temperatures may be measured by using either tipping curves directly or by using nominal hot load corrections based on tipping curves. Coefficients may be derived from brightness temperature data using a constrained regression analysis against radiosonde-measured path delays, or from a constrained regression analysis of theoretically calculated sky brightness temperatures against radiosonde measured path delays. The coefficients are functions of surface temperature, pressure, and water vapor density, to allow use of the data reduction algorithm at any altitude and in any climate.

[4]Three corrections should be made to Westwater's oxygen absorption coefficient. The pressure should be partial pressure of dry air only, except in the line width where it is total pressure. The coefficient of the line width should be changed to 0.025 from 0.049. The power law temperature dependence of the line width should be changed to 0.85 from 0.75 (Westwater, E. R., private communication).

Acknowledgements

We thank our colleagues, Joe Waters, Joe Stacey, and Bruce Gary, for valuable discussions regarding radiometer data reduction. Bruce Gary has been especially generous with his time and unpublished calculations made for a parallel program of atmospheric remote sensing. He suggested inclusion of temperature and pressure dependence in the inversion coefficients and brought our attention to the inaccuracy of coefficients derived by a simple least squares fit.

References

1. MacDoran, P. F., "Radio Interferometry for International Study of the Earthquake Mechanism," *Acta Astronautica*, Vol. 1, pp. 1427-1444, 1974.

2. Waters, J. W., "Absorption and Emission by Atmospheric Gases," in *Methods of Experimental Physics*, Vol. 12. New York: Academic Press, Chapter 2.3, 1976.

3. Wu, S. C., "Frequency Selection and Calibration of a Water Vapor Radiometer," *DSN Progress Report 42-43*, Jet Propulsion Laboratory, Pasadena, CA, pp. 67-81, Feb. 15, 1978.

4. Gunn, K. L., and East, T. W., "The Microwave Properties of Precipitation Particles," *Quart, J. Roy. Meterol. Soc.*, Vol. 80, pp. 522-545, 1954.

5. Klein, L. A., and Smith, C. T., "An Improved Model for the Dielectric Constant of Sea Water at Microwave Frequencies," *IEEE Trans. Anten. Prop.*, Vol. AP-25, pp. 104-111, Jan. 1977.

6. Crane, R. K., "Microwave Scattering Parameters for New England Rain," Lincoln Laboratory Technical Report 426, Lexington, MA, pp. 55-57, Oct. 1966.

7. Westwater, E. R., "An Analysis of the Correction of Range Errors Due to Atmospheric Refraction by Microwave Radiometric Techniques," U.S. Department of Commerce/ ESSA Tech. Report, IER 30-ITSA 30, Boulder, CO, Mar. 1967.

8. Thayer, G. D., "An Improved Equation for the Radio Refractive Index of Air," *Radio Science*, Vol. 9, pp. 803-807, 1974.

9. Smith, E. K., and Weintraub, S., "The Constants in the Equation for Atmospheric Refractive Index at Radio Frequencies," *Proc. IRE*, Vol. 41, pp. 1035-1037, 1953.

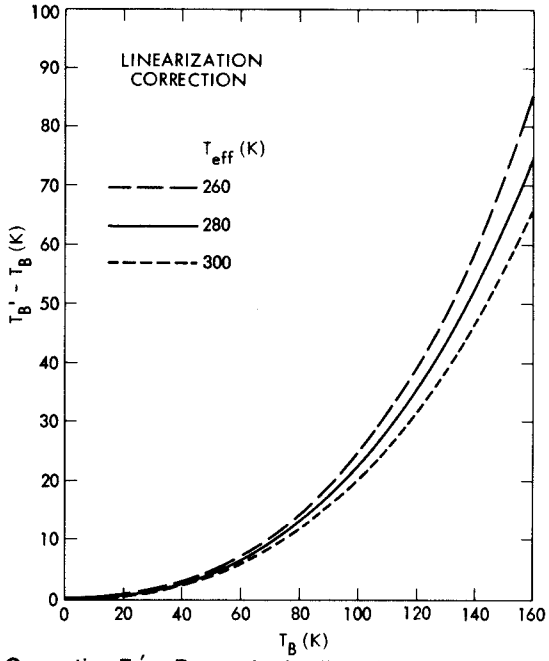

Fig. 1. Correction $T_B' - T_B$ required to linearize brightness temperatures T_B for three effective temperatures T_{eff}

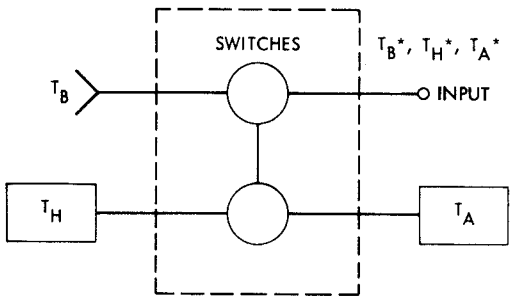

Fig. 2. Signal paths in a typical radiometer

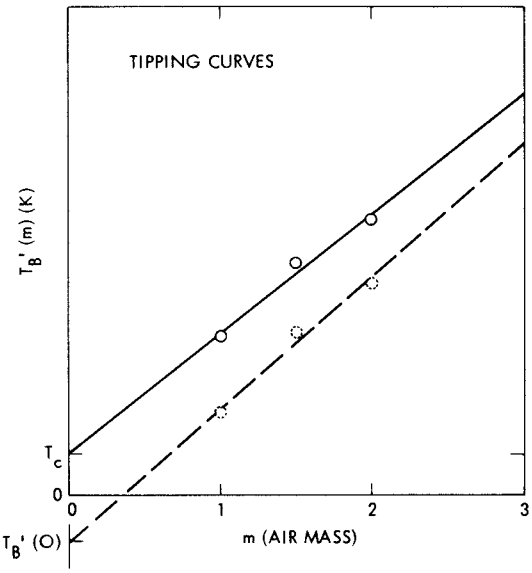

Fig. 3. Tipping curves with no hot load correction (dashed line) and with hot load correction required to give desired zero air mass intercept T_c (solid line); hypothetical data points for each case are also shown

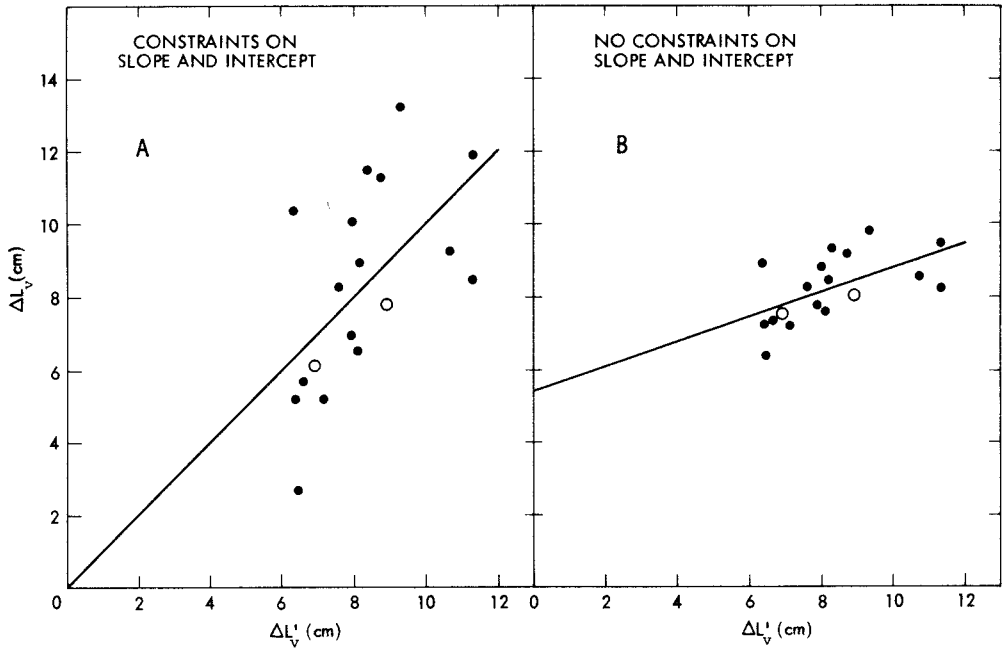

Fig. 4. Path delay ΔL_v from radiometer measurements vs path delay $\Delta L_v'$ from radiosondes using regression: (A) with constraints on slope and intercept, (B) without constraints on slope and intercept. A circle is used to indicate two overlapping points; the straight lines are least squares fits to the points generated by each regression